Experimental Analysis of the Source and Sink Relationship in a Meandering Bend

Li HE
Key Laboratory of Water Cycle and Related Land Surface Processes, Institute of Geographic Sciences and Natural Resources Research, Chinese Academy of Sciences, China
E-mail: heli@igsnrr.ac.cn

Abstract: The source-sink-relationships in natural rivers are compound results of various influencing factors, and correlated fitted equations are kind of qualitative description. Experiment analyses was conducted in a laboratory flume to reach a quantitative description, whose center line follows a sine-generated curve with deflection angle of 30 degree. Three-dimensional velocities, bed deformation and composition of the pool-bar complexes in the meander bend are analyzed. The comparison of deformed bed and the depth-averaged velocities founds that, the maximum depth-averaged velocities of sections around the transition reach occurred at the edge of pool with smaller transverse slope, and the maximum depth-averaged velocities for sections around the apex section occurred at the edge of pool with larger transverse slope. Quantitative analysis of the composition of pool-bar complexes revealed the source-sink relation of moved particles. It shows that, moved particles sourced from the concave bank are mainly come from area down the apex section, and moved particles sourced from the convex bank are mainly come from area upper the apex section. Besides, there exit an area with strong sediment exchange, namely the bar around the convex-side of the apex section.
Keywords: experimental flume; depth-averaged velocity; bed deformation; pool-bar complexes; source-sink relation

1. Introduction

Meanders are ubiquitous features of many alluvial rivers [1]. Understanding meandering river is important for a host of engineers and geologic applicators, as it is widely related to stream restoration and agriculture management [2]–[4]). Various researchers focus on meanders by field observation, experimental analysis (i.e., [5]–[8]) and numerical simulation (i.e., [9]). Despite these significant contributions on illustrating meandering river dynamics, failed restoration projects indicate limited understanding of the dynamic characteristics in meander rivers (relationship among flow structure and planform evolution) [1] .

The sediment sources and sinks in natural rivers are analyzed based on field investigation [10]–[11]. However, the source-sink-relationships in natural rivers are compound results of various influencing factors, velocity, bank materials, non-uniform sediment distribution of suspended sediment and bed material, planform of river meander, and et al.. The description is kind of qualitative, and may be expressed with a fitted equation. The purpose of this research is describing the source-sink relation of pool-bar complexes in a quantitative way by experimental data, by investigating the interactions among depth-averaged velocity field and planform evolution of meander bends. Experimental analyses in flume with stable banks are widely adapted to analysis the dynamic and the bed deformation (i.e., [6]). As in meander rivers, channel width and cross-sectional area remain about constant during the laterally migrating [12], even some researches stated that the width varies around an equilibrium width as lateral migration is discontinuous [12]. Erosion of the concave sides of meanders is matched by deposition of point bar material on the convex sides, and the source-sink-relation of pool-bar-complexes can be analyzed with reasonable design in a quantified way. So, experiment in a meander flume with fixed bank and colored particles is carried out. Flows passing through the meander on the scoured bed were measured, by using a micro ADV. Time histories of three-dimensional velocities were recorded at cross sections perpendicular to the centerline. These measurements were used to study time-averaged, downstream primary flow and cross-sectional flow properties. Then, bed material are collected and recognized, and distribution of colored particles of a scoured bed can be estimated, which reveals the source-sink relation of pool-bar complexes.

2. Experimental setup

Experiment was conducted in the laboratory of Institute of Geographic Sciences and Nature Resources Research, Chinese Academy of Sciences. The flume was installed on a basin equipped with a water recirculating system as shown in Fig. 1. A valve was used to control discharge in the inlet, and a sluice gate was used to control the water stage on the outlet. Both channel sides are plexiglass walls, and the thicknesses of floor and wall are 10 mm and 8 mm, respectively.

The centerline of the flume follows a sine-generated curve, and the deflection angle (θ_0) is 30 degree. The meander wavelength (Λ) is 2.518 m ($\Lambda = 2\pi B$), and the channel-length is 2.694 m (Fig. 1). This flume has rectangular cross sections with a constant width of 40 cm and a constant depth of 20 cm. The total extent of the channel (L_T) equals two meander lengths ($L_T = 2L$), and its first and last sections coinciding with apex-sections. The sinuosity δ is about 1.07. Two short transitional straight channels are connected with the upstream and downstream ends of the curved flume, and the lengths are 0.8 m and 0.6 m, respectively. One thing should be pointed out is that, the planform of the bend do not fit the features of freely meandering streams. For example, they do not fit the rule of meander length being about 10 times the width [13].

Water discharge was measured with a flowmeter (accuracy 0.01 L/minute). A micro ADV with side-looking probe was used to measure instantaneous velocity field. It can measure mean flow velocities from 1 mm/s to 2.5 m/s with an accuracy of ±1% of the measurement range. The transmit length is 2.4 mm. The sample volume is 9.1 mm, which located about 44 mm from the probe tip. The micro ADV was attached to a point gauge fixed on an instrument carriage that was mounted on horizontal steel rails and moved on wheels. So the ADV could move along the flume automatically driven by an electric motor, and it could also move manually in transverse and vertical directions to measure flow velocities at any location. The sampling frequency for the ADV was 20 Hz, with a sampling duration of 2-3 minutes in each measuring location. Different sampling frequencies for the ADV are adopted by various researches (i.e., [14]–[15]), and the recommended by Garcia et al. [16] is 100 Hz. Analysis showed that, 180 s of sampling yield stationary results for all measuring points including them in the shear layer zone [17]. Measurements with higher sampling rate showed the contribution of higher Doppler noise in time series.

The channel bed consisted of well-sorted silica sand having an average grain size (mean diameter D_{50}=1mm). And the specific density of the sand was 2.65. As shown in Fig. 1, bend B_1 and B_2 are paved with colored particles, and the rests of the flume are paved with white particles with same diameter. Dividing by central stream line, particles paved in the left side and right side of bend B_1 and B_2 are different (Fig. 1). So, there are four colored particles initially paved in bend B_1 and B_2, named as D_1, D_2, D_3 and D_4, respectively. Particles of D_1 and D_2 are initially paved in the concave side, and particles of D_3 and D_4 are initially paved in the convex side. The water temperature is about 14℃.

The run started from a bed having zero radial slope and a specified longitudinal slope S_{bc} (flat initial bed at t = 0). And the channel bed slope (S_{bc}) paved by particles was 0.0001. At the beginning of the runs, the water elevation at the downstream-end of the meandering channel was set (with the aid of a tailgate) so that the free surface slope S_w was identical to the slope of the flat initial bed S_{bc} ("uniform" flow conditions). Constant water depth was maintained by the tailgate. Small adjustments to the position of the tailgate were occasionally required during the runs to maintain $S_w \approx S_{bc}$ throughout the duration of the runs. Sediment accumulating in the sand collection reservoir was not re-circulated. To prevent any disturbance of the bed, water was not injected as a point source, and it flowed smoothly onto the river bed via a transition reach (see Fig. 1). Bed topography was generated by a steady water discharge.

The measuring points of bed formation and velocities are different. For measuring bed formation of the curved channel with half meandering wavelength, there are nine cross-sections and fifteen vertical profiles at intervals of 5 cm (solid dots in Fig. 2). Flow moving through simple meander bends is highly three dimensional [18], and three-dimensional velocities are measured with micro ADV. For measuring velocities of the curved channel with half meandering wavelength, there are five cross-sections and seven vertical profiles at intervals of 5 cm (hollow squares in Fig. 2). Each vertical profile had one to eleven points with 1cm spacing, and the amount of points depends on the equilibrium bed formation. The maximum amount of measuring node in vertical profile is 11 points (i.e., Sec15 with n=5 cm and n=10 cm), and the minimum amount is located at Sec 15 with n=30 cm. Totally, there are 228 measuring points with measured velocities. At each measuring node, about 2000 instantaneous velocities at three respective directions were recorded.

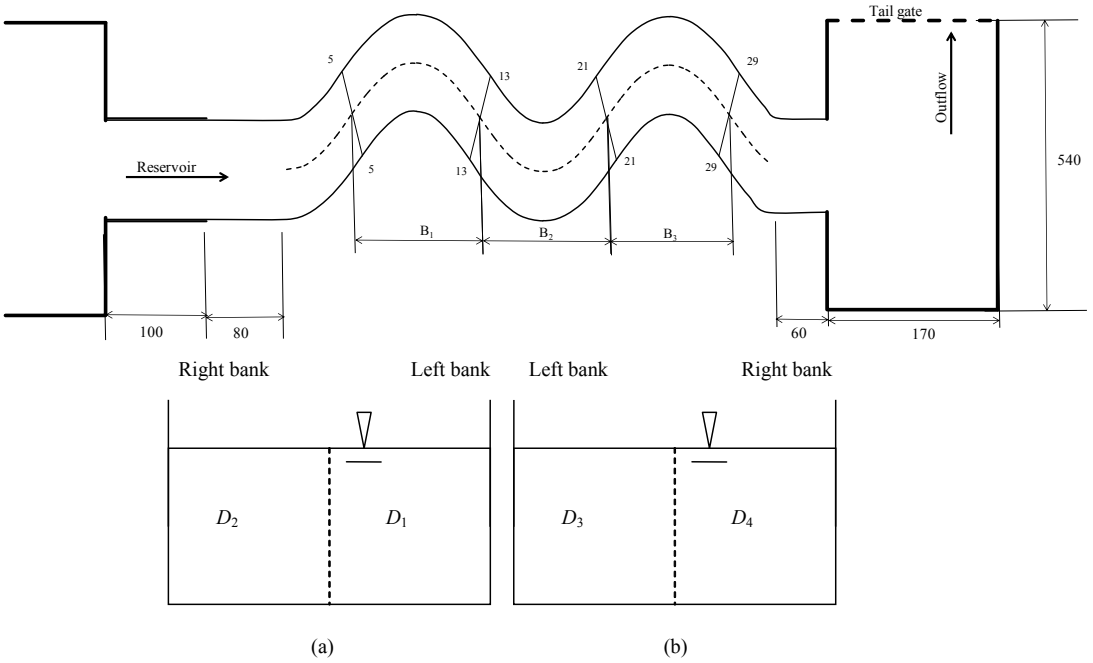

Fig. 1 Experimental setup and initial distribution of bed material in the numerical model (units are cm). For the plane distribution of bed materials with different colors (reach between Sec 5 and Sec 21), (a) is side-view of Sec 13 from downstream to upstream; and (b) is side-view of Sec 13 from upstream to downstream. Flow is from left to right

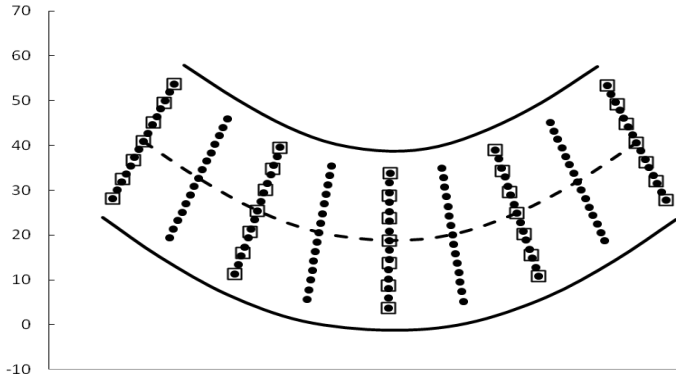

Fig. 2 Plan view of the bend with measurement points, solid dots for measurements of deformed bed, empty squares for measuring velocity. Flow is from left to right

3. Data Processing

The coordinate system used is cylindrical coordinate system. The origin of the cylindrical coordinate system located at the right side wall of the downstream face of the bend and at the initial flume bottom, with a streamwise axis (*s*) along the channel centerline, cross-stream *n*-axis normal to *s* positive in the left direction, and *z* axis toward to the water surface vertically. The Z=0 plane was at the initial bed surface. The velocity components were denoted as *U, V* and *W*, respectively. The approaching velocity is about 15.33 cm/s, with a discharge of 6.94 l/s.

There is some uncertainty associated with raw ADV data [19]. The time series are usually affected by Doppler noise, velocity shear inside the sampling volume, electronic errors and other Doppler signal interferences, all these influences may lead to spikes [19]. All of the measured raw velocity time series are processed to remove the influences of these errors, and mean values and turbulence statistics can be drawn. Following the manufacturer's instructions, the time series was filtered to reject points with average correlation score less than

70%, average SNR (Signal to Noise Ratio) less than 10dB, acceleration of spike filter less than 1g and clean up points with velocity threshold of 3 sigma.

At the upstream uniform flow reach, the friction velocity and roughness height were calculated by curve fitting the velocity profiles with the logarithmic law, using the velocity data in several vertical lines in the inlet cross section. With wall effect, the maximum mean-velocity U occurred slightly below the free surface, indicative of dip phenomenon when the rectangular channels have a low flow aspect ratios ($B/H \leq 5$) [20]. And the dip phenomenon is not very significant when measurements are made in the center of the channel and the flow aspect ratio is large [20]. The channel-averaged flow depth is about 5.6 cm, and the corresponding width-to-depth ratio in this experimental flume is 7.14. The aspect ratio herein is in the lower part of values by former experiments (ranging from 1.6 and 33.7) [21].

The shear velocity was determined by fitting the logarithmic velocity distribution while assuming the von Karman constant is 0.41. Then the thickness of viscous sublayer $\delta=11.6v/u_*$, Reynolds number of incoming flow R, and the mean velocity of approaching flow U_0 could be calculated accordingly. The shear velocity was $u_*=2.07\ cm/S$ and the roughness height was $ks=1mm$, which was much greater than the thickness of viscous sublayer $\delta=11.6v/u_*=0.56\ mm$. Therefore, flow was hydraulically rough, with Reynolds number of 8584. And the Froude number is 0.207.

4. Results and discussion

4.1 Equilibrium bed formation

The duration of the experimental run was more than 72 hours to allow the local scour reach an asymptotic state when no changes in bed elevation occurred and scouring was stopped. The inner assumption is that, the duration of experiment was sufficiently long to ensure the establishment of equilibrium conditions for the measurements of the bed topography. Contour lines of the scoured depth were shown in Fig. 3, and the zero contour line was the initial mobile bed surface indicating the edge of the scouring hole. The maximum scour depth is approximately 5.19 cm, locating at Sec 20 and 26.3cm from the right wall. Fig. 3 shows the bed formation in bend B_2, and the bed formations of the three bends are similar [22]. It means that, the zone of maximum deposition around the convex bank extends to the concave bank of the next bend.

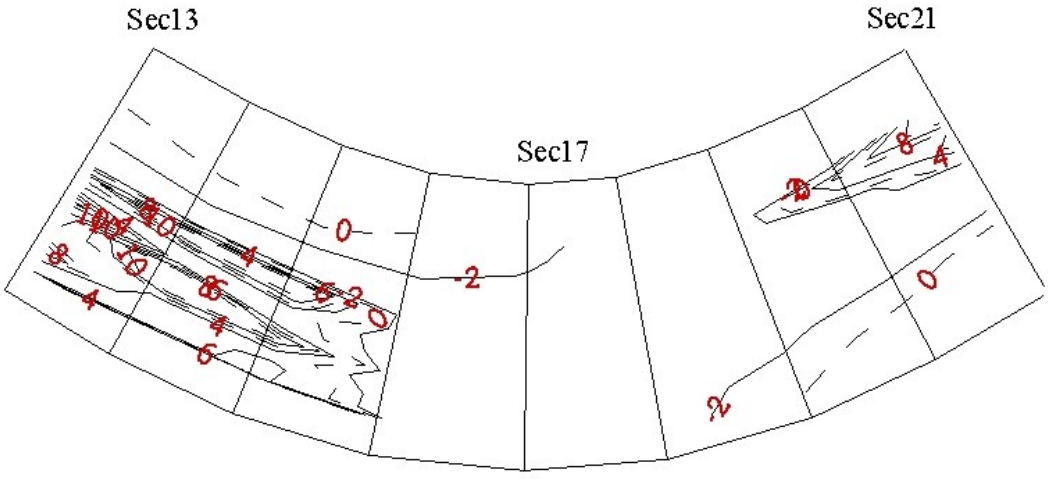

Fig. 3 Contour lines of bed elevation in bend B_2. The labels are the depth of erosion or deposition, with unit of cm. Flow is from left to right

The bend can be divided into three segments according to the bed deformation (Fig. 4). The first area is characterized with bar around the right bank (or say concave bank), and the pool begin to appear, and the pool is around the bend centerline. The second area is characterized with diminished bar around the concave bank and enhanced pool, and the pool extends cross the whole sections. The maximum depth of the pool is almost constant from Sec 13 to Sec 19. And the transverse slope decreases from 13.5% (Sec 16) to -13.3% (Sec 19). The third area is characterized with two bars and one pool. The bar around the right bank is relatively small (concave bank). The bar around the left bank is almost the same as the bar around Sec 13 and Sec 15. As the experiment bend is composed of three consecutive bends, and there are another two bends connected with the studies reach in the up- and down-stream, respectively. So, bar around Sec 20 and Sec 21 can be view as the initial part of bar around Sec 13 and Sec 15. It means that, the bar stars at sections down the apex section around the convex bank, and it ends before the apex section around the concave bank of bend followed. So, the area of bar in this flume extends crossing the transition section, from the upper bend to the followed bend. As the lateral bed slop is due to

an overshoot effect induced by the redistribution of the water and sediment motion [6]. Jamieson et al. [23]–[24] performed laboratory flow measurements around stream barbs (submerged groynes) in a curved channel at equilibrium clear-water condition. Based on turbulence and vorticity fields analysis, they found that increased streamwise cross- stream Reynolds stress coincide with locations of the scour hole [23]–[24]. It means that, the locations of the scour hole are the place where redistribution of water and sediment motion and the streamwise cross- stream Reynolds stress occurred.

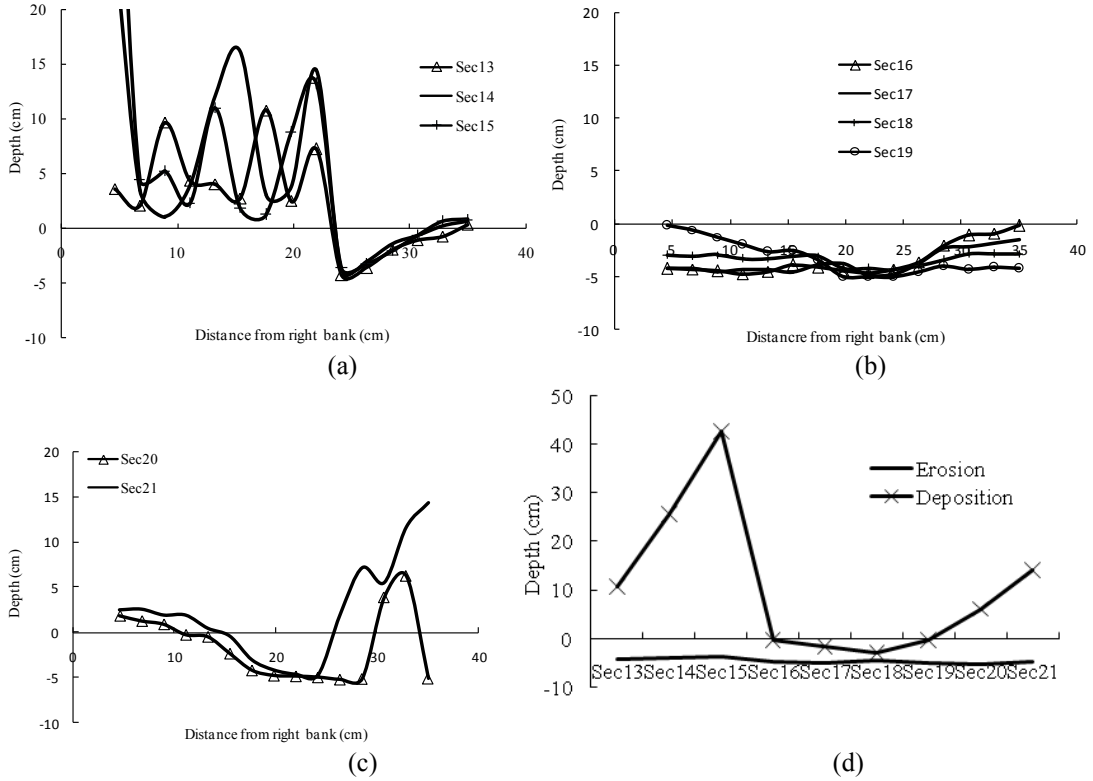

Fig. 4 Geometry of cross sections in the bend, (a) area with bar around the right side; (b) area with cross-sectional pool, (c) are with bar around the left side; and (d) longitudinal distribution of maximum erosion depth and deposition depth

Pyrce and Ashmore [25] pointed out that, sediment is deposited on the point bar firstly, and the changed bed form causes more erosion of the outer bank. During the process of bed formation of equilibrium bed herein, the acceleration of point bar is relatively more visible. The first stage is deposition around the convex bank at section down the apex section. Then, the bar may move gradually along the same side. It may move cross the transition section, and come up to apex section around the concave bank. The movement of the front of the bar slowed after it reaches Sec 15, and it stops at section before Sec 16. However, sank particles are sourced from upper stream or the other bank, so, the source-sink-relation of pool-bar-complexes can be analyzed by sampling of the experimental flume.

4.2 Depth-averaged velocities

The depth-averaged velocities and the deformed bed are shown in Fig. 5. It shows that, the bar may shift the flow toward the other bank. Besides, the zone of maximum deposition coincides with the zone of spiral vortices [26]. Depth-averaged velocities show that, the vortex around the apex section is relatively limited (i.e., the left bank of Sec 19–21).

The transversal distributions of depth-averaged velocities are shown in Fig. 6. At Sec 13, the depth-average velocities around the bar are almost the same (larger than 17 cm/s), and it decreases dramatically around the left bank (about 5 cm/s). At Sec 15, the depth-average velocity at vertical profile of n=15 cm (about 15 cm/s) is the smallest except the profile of n=35 cm (about 3 cm/s). For these two cross sections, the depth-averaged velocities around the bar are relatively larger, and the profiles with minimum depth-averaged velocities are profiles with n=35 cm where limited deposition occurred. The profiles with minimum velocities at Sec 13 and Sec 15 located near the left bank, while these profiles changed to the right bank downstream of Sec 17, and it moves back to the left bank after the apex section (i.e., Sec 19 and Sec 21).

The transversal distributions of Sec 15 and Sec 21 show that, the profiles with maximum depth-averaged velocities occurred at the edge of pool with smaller transverse slope (with Z=0). For Sec 17 and Sec 19, the profiles with maximum depth-averaged velocities occurred at the edge of pool with larger transverse slope.

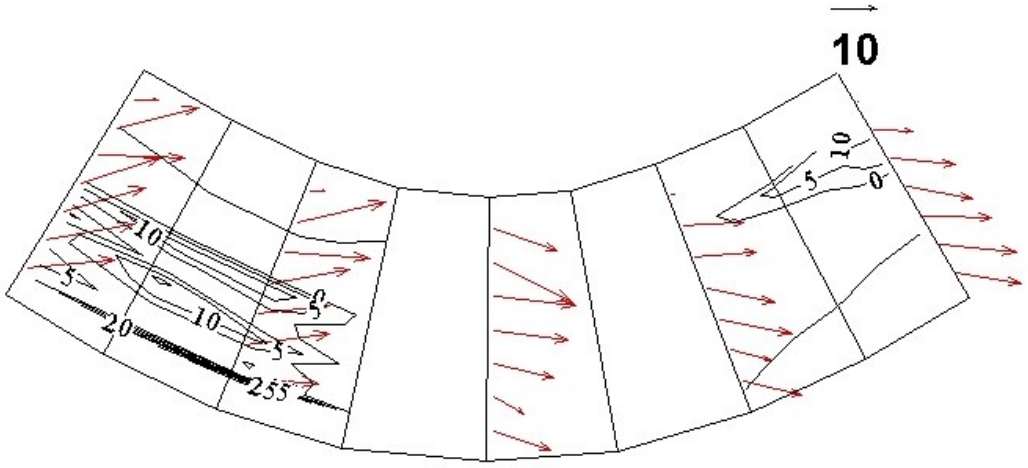

Fig. 5 Plan distributions of depth-averaged velocities and corresponding deformed bed in bend B_2. Flow is from left to right

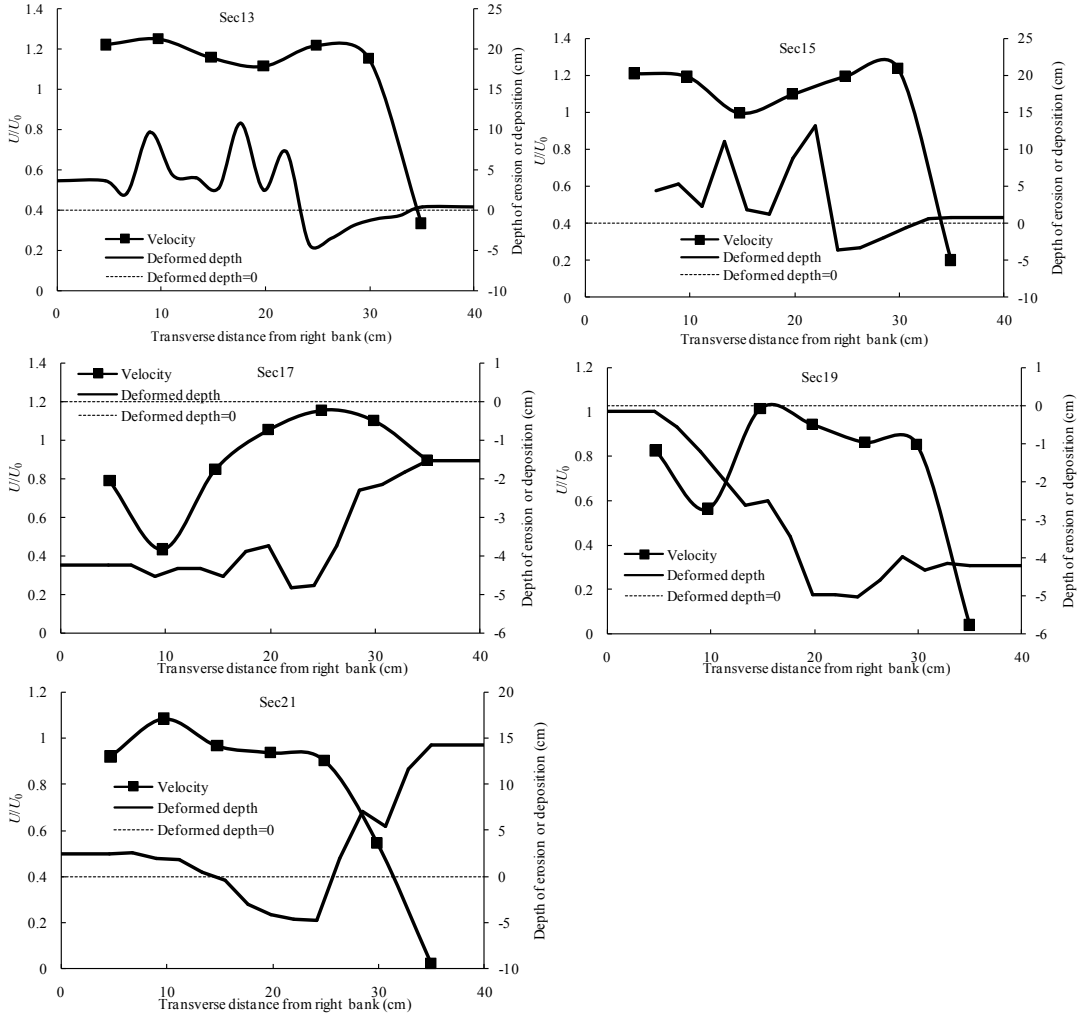

Fig. 6 Comparison of dimensionless velocity and corresponding geometry of cross-sections along the bend

4.3 Plane distribution of velocities and deformed bed

The plain distribution of depth-averaged velocities and bed formation are illustrated in Fig. 7. The maximum depth-averaged velocity at Sec 13 is about 19.2 cm/s, which is located on the right side of the top of the bar. Fig. 7 shows that, the maximum depth-averaged velocity of Sec 13 is around the right bank of the bend. Then, it turns toward the left bank, and the maximum depth-averaged velocity of the apex section turns toward the right bank.

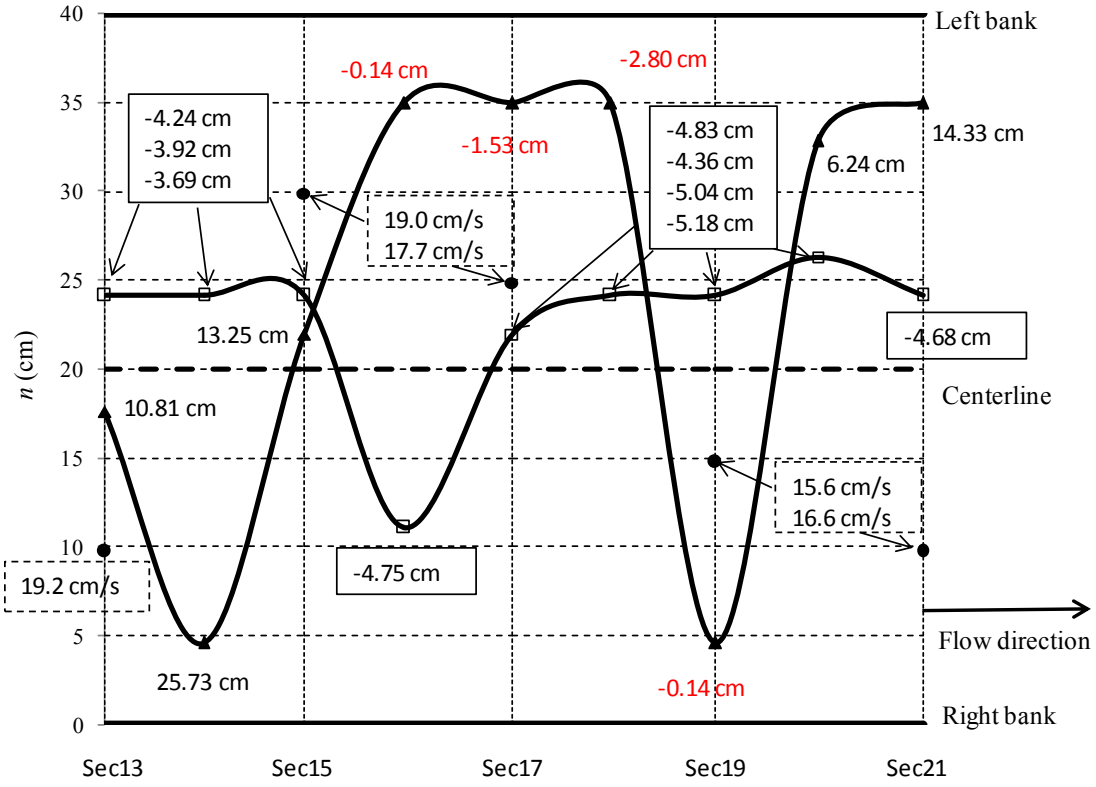

Fig. 7 Plane distributions of points with maximum and minimum bed deformation and maximum velocities in s-direction. Solid triangular demonstrate locations of points with the largest value of bed deformation in each cross-section, and the corresponding values are the magnitude of changed bed elevation. Red values indicate that, the bed-elevation between Sec 16 and Sec 19 decreased by erosion. Hollow squares demonstrate locations of points with the smallest value of bed deformation in each cross-section, and the corresponding values are the magnitude of changed bed elevation, which are listed in box with solid lines. Solid dots demonstrate locations of points with the largest longitudinal velocity in each cross-section, and the corresponding values are the magnitude of velocity, which are listed in box with dashed lines. Flow is from left to right

According to the depth-averaged velocities illustrated in Figs. 5 to 7, the main flow can be identified (Fig. 8). For Sec 13, the depth-averaged velocities around the bar is almost the same, and the profile with maximum velocities is identified at the location of n=25 cm to making a smooth line. And the corresponding velocity is 18.7cm/s. Comparing to the maximum velocity of 19.2 cm/s, the velocity of the identified main flow is about 2.6% smaller. So, the smoothed main flow is reasonable. Comparing to the lotus of maximum bed shear stress in Engel [1], the locus of high velocity in Parker [27], and the lotus of the coarse material in Parker and Andrews [28], the locus of main flow is almost the same as that three lotuses, except the point where it moves cross the centerline. It means that, the shift of main flow herein occurred at section relatively downstream of the apex section.

At sections upper the apex section, the maximum sediment flux occurred around the convex bank but close to the centerline, and at sections down the apex section, the maximum sediment flux moves much more close to the convex bank [29]. In total, the locus of maximum sediment flux goes along the convex bank. According to the locus of coarse material illustrated in Parker and Andrews [28], particles located at section upper the apex section around the convex bank may be moved across the centerline toward the concave bank. Moreover, the amount of sediment eroded from the concave bend is in most cases approximately equal to the amount of sediment deposited on the convex bank [13].

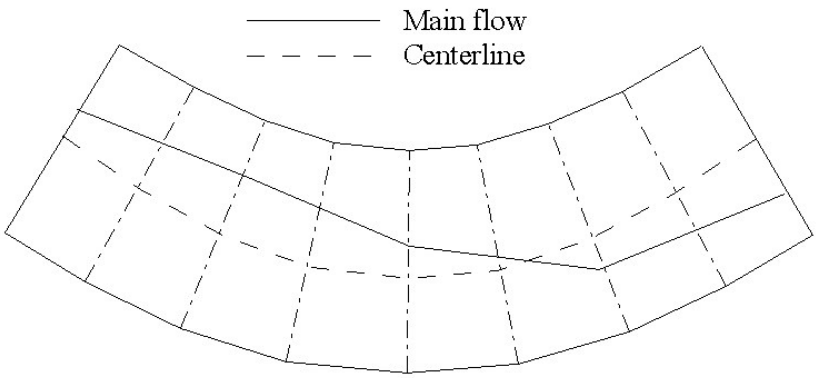

Fig. 8 Diagram illustrating of locus of high velocity in bend B_2. Flow is from left to right

4.4 Composition of pool-bar complexes in the bend

By distinguishing the colored particles, the composition of pool-bar complexes can be identified. The components of pool-bar complexes in bend B_2 are illustrated in Fig. 9. As the convenient of sampling, the pool-bar complexes are not seriously distinguished. The sampling zones in the longitudinal direction are divided by cross sections where velocities are measured (shown in Fig. 2). And there are four samples in the transverse direction, which are equally divided. It means that, there are two samples both on the left and right side of the centerline. According to the principle of sampling zone division, the sampling areas of all these samples are almost the same, the width of all the samples are exactly the same, and the length of all the samples are almost the same.

The plan distributions of D_2 and D_3 in Fig. 9 indicate a cross-centerline kind of source-sink pattern. And former flume experiments indicate that, eroded particles originally located at the concave bank can across the channel centerline and move towards the opposite bank [31]. The plan distributions of D_1 in Fig. 9a and D_4 in Fig. 9b indicates kind of same-bank source-sink pattern. Former field observation and experiments also found that, most particles eroded from a concave bank transport along the same-side bank and deposit at the convex bank as point bar of the next bend, rather than across the centerline and deposit at the opposite bank [32]–[34].

Fig. 10 illustrates the ratio of each group of particles. According to the bed deformation in Fig. 3 and the distribution of source-sink pattern in Fig. 9, the two pools are discussed as a whole. Particles moved from local means particles from the same side of the pool or bar. Local bend means the other side of the bend where the pool or bar is located, and sediment sank from local bend means sediment across the channel centerline in the local bend. Particles from upper bend mean the contribution of the whole upper bend, including both the left side and right side. Fig 10 indicates that, moved particles sourced from the concave bank are mainly come from area down the apex section, and the corresponding sink area is mainly the next bend. Field observation by Mathes [32] and experiments by Friedkin [33] also indicate that, most particles eroded near a concave bank transport along the same-side channel bank and deposit at the downstream point bar of the next bend, rather than across the centerline and shape the present point bar on the opposite side of channel. Moved particles sourced from the convex bank are mainly come from area upper the apex section, and the corresponding sink area is mainly the next bend. Experiments by Wang [34] also indicate that, bed material deposited at a point bar mainly comes from upstream rather than from the opposite bank. The smaller ratios of sank particles from local bend (both of pools and bars) indicates limited transverse movement, as sediment across the channel centerline only in highly sinuous channels which is proposed by Zhang and Lv [35]. The secondary flow highly depends on the width-to-depth ratio [36], and the aspect ratios (B/H) herein is 7.14, which is much smaller than that in natural rivers [37]. The 'helix strength' increases as the ratio B/H decreases [38], and the 'helix strength' in flume is relatively larger than that of natural rivers.

The volume of the convex-bar around the apex section is limited, but the particle exchange is obvious. A great part of particles moved out of the area, and almost a similar part of particles sank from the upper bend. The sediment flux at section downstream of the apex section around the convex bank is the largest [29].

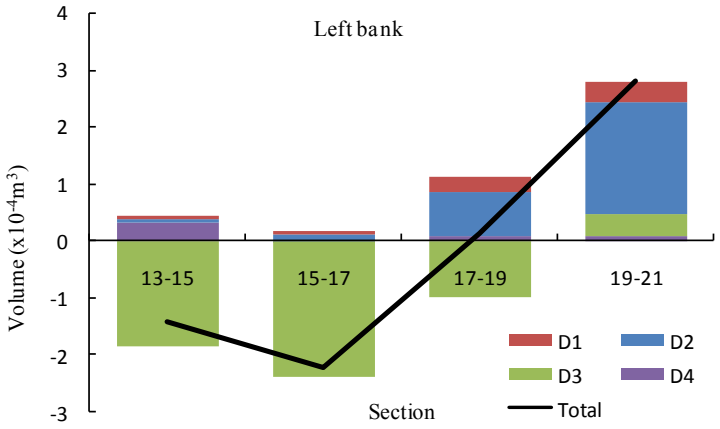

(a) Left side of the centerline, the convex bank

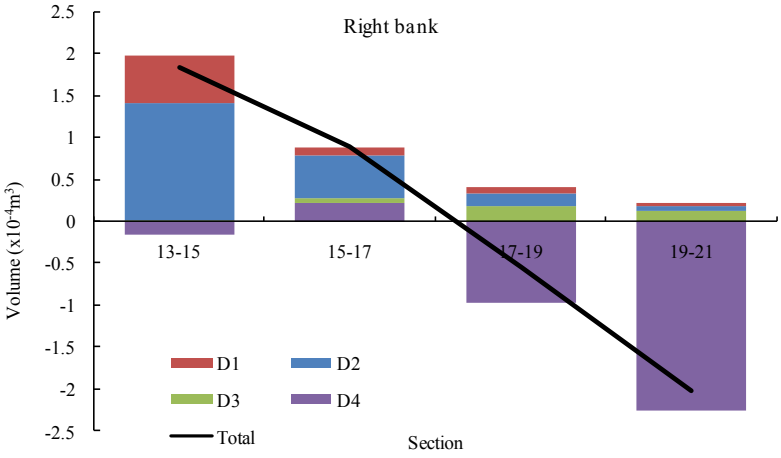

(b) Right side of the centerline, concave bank

Fig. 9 Component of all samples in bend B_2

However, the importance of transverse sediment fluxes remains a debut, being primarily responsible for the growth of sand bars and erosion of concave banks [39], or being overestimated transverse transportation in meanders [40]. As meanders migrate, sinuosity and curvature tend to increase, forming elongate bends with multiple curvature maximums [1]. So, future arrangement should be experimental and numerical analyses with different experiment parameters (i.e., flection angel, large-amplitude, sediment size, slope and discharge rate).

5. Conclusion

Based on bank-restricted meander bend with small amplitude, the depth-averaged velocities, bed deformation and the composition of the pool-bar complexes are quantitatively analyzed. Several finds can be drawn,

(1) For sections around the transition reach, the maximum depth-averaged velocities occurred at the edge of pool with smaller transverse slope, and the maximum depth-averaged velocities for sections around the apex section occurred at the edge of pool with larger transverse slope.

(2) Moved particles sourced from the concave bank are mainly come from area down the apex section, and moved particles sourced from the convex bank are mainly come from area upper the apex section. The corresponding sink areas of concave-bank-sourced and convex-bank-sourced particles are the next bend.

(3) The experiment flume analysis revealed an area with strong sediment exchanged, and the area is the bar around the convex-side of apex section. A great part of particles moved out of the area, and almost a similar part of particles sank from the upper bend.

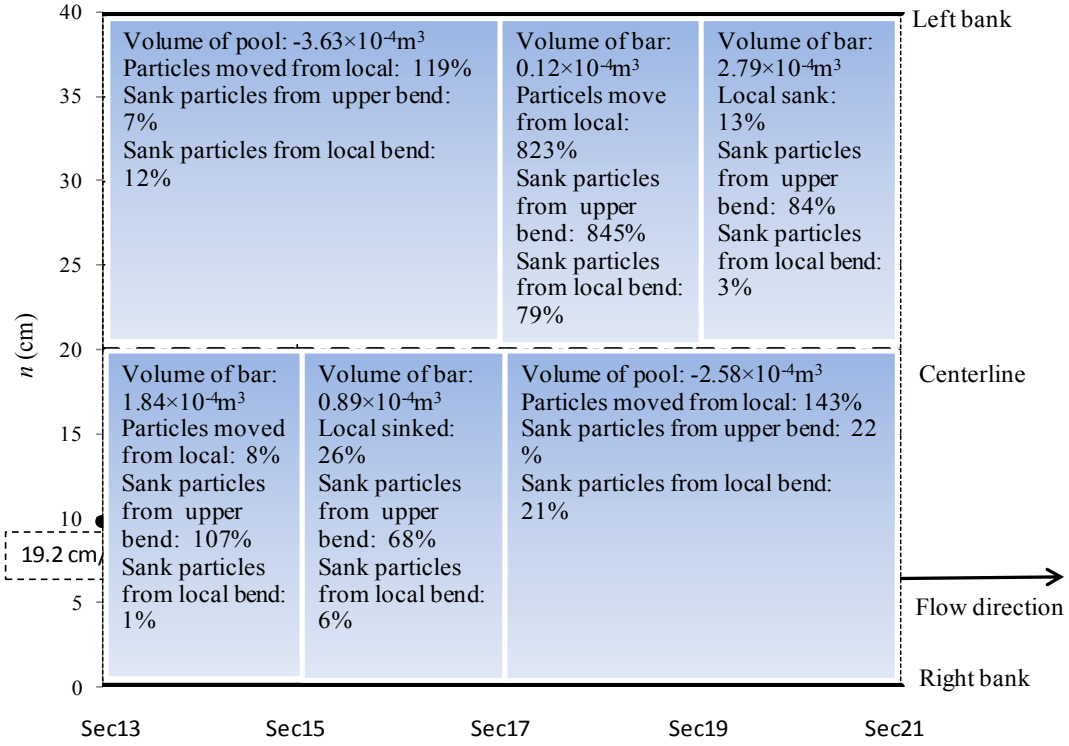

Fig. 10 Sketch maps of the source and sink of pool-bar complexes in bend B_2. Flow is from left to right

Acknowledgement

This research was supported by (1) the National Natural Science Foundation of China (No. 51579230), (2) the National Natural Science Foundation of China (No. 41571005, 51109198), and (4) the National Science and Technology Support Program (No. 2012BAB02B02, 2011CB403305).

References

[1] Engel, F. The fluvial dynamics of compound meander bends. University of Illinois. 2014.

[2] Schwenk, J., Lanzoni, S., Foufoula-Georgiou, E. The life of a meander bend: Connecting shape and dynamics via analysis of a numerical model. J. Geophys. Res. Earth Surf., 2015. 120: 690–710. doi: 10.1002/2014JF003252.

[3] Van de Lageweg, W. I., van Dijk, W. M., Kleinhans, M.G. Channel belt architecture formed by a meandering river. Sedimentology, 2013. 60(3): 840–859. doi:10.1111/j.1365-3091.2012.01365.x.

[4] Beschta, R.L., Ripple W.J. The role of large predators in maintaining riparian plant communities and river morphology. Geomorphology, 2012. 157: 88–98, doi:10.1016/j.geomorph.2011.04.042.

[5] Riley, J.D., Rhoads, B.L. Flow structure and channel morphology at a natural confluent meander bend. Geomorphology, 2012: 163–164.

[6] Struiksma, N., Flokstra, C. Bed deformation in curved alluvial channels. Journal of Hydraulic Research, 1985. 23(1): 57–79.

[7] Chen, D., He, L., Liu, J. Experimental study on sediment transport in meander channels. AGU fall meeting abstracts, 2013.

[8] Termini, D. Experimental observations of cross-sectional flow motion in a large amplitude meandering bend. Earth Surface Processes and Landforms, 2011. 36: 244–256.

[9] Chen, D., Duan, J.D. Simulating sine-generated meandering channel evolution with an analytical model. Journal of Hydraulic Research-IAHR, 2006. 44(3): 363–373.

[10] Stout, J.C., Belmont, P., Schottler, S.P., Willenbring, J.K. Identifying Sediment Sources and Sinks in the Root River, Southeastern Minnesota. Annals of the Association of American Geographers, 2014. 104:1, 20–39, DOI: 10.1080/00045608.2013.843434.

[11] Kocurek, G., Ewing, R.C. Source-to-sink: An earth/mars comparison of boundary conditions for Eolian Dune systems. 2012.

[12] Nanson, G.C., Hickin, E.J. Channel migration and incision on the Beatton River. Journal of Hydraulic Engineering-ASCE, 1983. 109: 327–337.

[13] Leopold, L.B., Wolman, M.G. River meanders. Bulletin of the Geological Society of America, 1960. 71: 769–94.

[14] Duan, J.G., He, L., Fu X.D., Wang. G.Q. Mean Flow and Turbulence around Experimental Spur Dike. Advances in Water Resources, 2009. 32(12): 1717–1725. doi:10.1016/j.advwatres.2009.09.004.

[15] Yarahmadi, M.B., Bejestan, M.S. Sediment management and flow patterns at river bend due to triangular vanes attached to the bank. Journal of Hydro-environmental Research, 2016. 10: 64–75.

[16] Garcia, C.M., Cantero, M.I., Nino, Y., Garcia, M.H. Turbulence measurements with acoustic Doppler velocimeters. Journal of Hydraulic Engineering-ASCE, 2005. 131: 12(1062), 1062–1073. 10.1061/ (ASCE) 0733-9429(2005)

[17] Safarzadeh, A., Neyshabouri, S.A.A.S., Zarrati, A.R. Experimental investigation on 3D turbulent flow around straight and T-shaped groynes in a flat bed channel. Journal of Hydraulic Engineering-ASCE, 2016. 142(8): 04016021.

[18] Da Silva, W.E. Mechanics of flow and sediment transport in river bends. In River channels environment and process, ed. K. S. Richards, Oxford: Basil Blackwell. 1987: 179–224.

[19] Togneri, M.; Lewis, M.; Neill, S.; Masters, I. Comparison of ADCP observations and 3D model simulations of turbulence at a tidal energy site. Renew Energ., 2017. 114: 273–282.

[20] Balachandar, R., Bhuiyan, F. Higher-order momentums of velocity fluctuations in an open-channel flow with large bottom roughness. Journal of Hydraulic Engineering-ASCE, 2007. 133(1): 77–87.

[21] Termini, D., Poraino, M. Experimental analysis of cross-sectional flow motion in a large amplitude meandering bend. Earth Surface Processes and Landforms, 2011. 36: 244–256.

[22] Binns, A.D., da Silva, A.M.F. Rate of growth and other features of the temporal development of pool-bar complexes in meandering streams. Journal of Hydraulic Engineering-ASCE, 2011: 1565–1575.

[23] Jamieson, E., Rennie, C., Townsend, R. 3D flow and sediment dynamics in a laboratory channel bend with and without stream barbs. Journal of Hydraulic Engineering-ASCE, 2013: 154–166. 10.1061/ (ASCE)HY.1943-7900.0000655.

[24] Jamieson, E., Rennie, C., Townsend, R. Turbulence and vorticity in a laboratory channel bend at equilibrium clear-water scour with and without stream barbs. Journal of Hydraulic Engineering-ASCE, 2013: 259–268. 10.1061/(ASCE) HY.1943-7900.0000673.

[25] Pyrce, R., Ashmore, P. Bedload path length and point bar development in gravel-bed river models. Sedimentology, 2005. 52: 167–187.

[26] Leeder, M.R., Bridges, P.H. Flow separation in meander bends. Nature, 1975. 253(5490): 338–339.

[27] Parker, G. On the time development of meander bends. J. Fluid Mech., 1986. 162: 139–156.

[28] Parker, G., Andrews, E.D. Sorting of bed load sediment by flow in meander bends. Water Resources Research, 1985. 21(9): 1361–1373.

[29] Palmsten, M.L., Kozarek, J.L., Calantoni, J. Video observation of bed form morphodynamics in a meander bend. Water Resources Research, 2015: 7238–7257.

[30] Kleinhans, M.G., Blanckaert, K., Mclelland, S.J., Uijttewaal, W.S.J., Murphy, B.J., Van de Kruijs, A., Parsons. D.R. Flow separation in sharp meander bends. In Proceedings of the HYDRALAB III Joint User Meeting. Hanover, Germany. 2010.

[31] Engels, H. Das Flussbau- Labora Torium DerkgL. Techni Schen Hochschule in Dresden, Derlin. 1900.

[32] Mathes, G.H. Basie aspects of Stream Meanders. Trans. Amer. GeoPhys Union, 1941. Pt. 111.

[33] Friedkin, J. A laboratory study of the meandering of alluvial rivers. US Waterways Experiment Station: Vicksburg. 1945.

[34] Wang, B. Experiments of water flow and bed deformation in a flume with consecutive curves. Tsinghua Univ., Beijing, China. 2008. (in Chinese)

[35] Zhang, H.W., Lv, X. Bend hydraulics. Beijing: Water Conservancy and Electric Power Press. 1993. (in Chinese)

[36] Termini, D. Momentum transport and bed shear stress distribution in meandering bend: experimental analysis in a laboratory flume. Advance in Water Resources, 2015. 81: 128–141.

[37] Dolgopolova, E.N. The coefficient of friction in channel flow. Water Resources, 2000. 27(6): 611–616.

[38] Hooke, R.L.B. Distribution of sediment transport and shear stress in a meander bend. J. Geol., 1975. 83(5): 543–566.

[39] Nouh, M., Townsend, R. Shear stress distribution in stable channel bends. J. Hydr. Div.-ASCE, 1979. 105(10): 1233–1245.

[40] Pittaluga, M.B., Seminara, G. Nonlinearity and unsteadiness in river meandering: a review of progress in theory and modeling. Earth Surface Processes and Landforms, 2011. 36(1): 20–38.